Engineering Nanoscale Thermal Transport: Size- and Spacing-Dependent Cooling of Nanostructures

Travis D. Frazer,[1,*] Joshua L. Knobloch,[1] Kathleen M. Hoogeboom-Pot,[1] Damiano Nardi,[1] Weilun Chao,[2] Roger W. Falcone,[3] Margaret M. Murnane,[1] Henry C. Kapteyn,[1] and Jorge N. Hernandez-Charpak[1]

[1] *JILA and Department of Physics, University of Colorado, Boulder, Colorado 80309, USA*
[2] *Center for X-Ray Optics, Lawrence Berkeley National Laboratory, Berkeley, California 94720, USA*
[3] *Department of Physics, University of California, Berkeley, California 94720, USA*

(Received 29 August 2018; revised manuscript received 19 November 2018; published 15 February 2019)

Nanoscale thermal transport is becoming ever more technologically important with the development of next-generation nanoelectronics, nanomediated thermal therapies, and high efficiency thermoelectric devices. However, direct experimental measurements of nondiffusive heat flow in nanoscale systems are challenging, and first-principle models of real geometries are not yet computationally feasible. In recent work, we used ultrafast pulses of short-wavelength light to uncover a previously-unobserved regime of nanoscale thermal transport that occurs when the width and separation of heat sources are comparable to the mean free paths of the dominant heat-carrying phonons in the substrate. We now systematically compare thermal transport from gratings of metallic nanolines with different periodicities, on both silicon and fused-silica substrates, to map the entire nanoscale thermal transport landscape – from closely spaced through increasingly isolated to fully isolated heat-transfer regimes. By monitoring the surface profile dynamics with subangstrom sensitivity, we directly measure thermal transport from the nanolines into the substrate. This allows us to quantify for the first time how the nanoline separation significantly impacts thermal transport into the substrate, making it possible to reach efficiencies that are within a factor of 2 of the diffusive (i.e., thin-film) limit. We also show that partially isolated nanolines perform significantly worse, because cooling occurs in a regime that is intermediate between close-packed and fully isolated heat sources. This work thus confirms the surprising prediction that closely spaced nanoscale heat sources can cool more quickly than when far apart. These results show that our predictive model is validated by experiment over a broad parameter space, which is important for benchmarking theories that go beyond the Fourier model of heat diffusion, and for informed design of nanoengineered systems.

DOI: 10.1103/PhysRevApplied.11.024042

I. INTRODUCTION

Advancing technology through nanoengineering often requires an understanding of how nanoscale thermal transport differs from its bulk counterpart. In modern electronics, characteristic dimensions are already below 10 nm – thus, thermal load management is already facing challenges imposed by nanoscale thermal transport. In medicine, nanoparticle-mediated thermal therapies are being developed to treat cancer and tumors with localized heating of those cells [1,2]. Additionally, nanostructuring is a promising avenue to engineer advanced materials for efficient thermoelectric devices, either through enhanced scattering [3,4] or through coherent effects [5–7]. For these and many other applications, informed design must take into account that nanoscale thermal transport can be significantly slower than bulk model predictions.

Fourier's law of heat conduction, which accurately describes thermal transport in bulk materials, relies on the fundamental assumption that the distances being considered are much larger than the average mean free path (MFP) of heat carriers in the system, therefore establishing a smooth thermal gradient that drives transport in a material. As a result, when the relevant length scale of thermal transport is on the order of the MFP of the heat carriers, Fourier's law is no longer accurate because it dramatically overpredicts the heat transfer rate [8]. In this regime, some of the heat carriers travel ballistically from the heat source and deposit their energy nonlocally, producing nondiffusive (quasiballistic) thermal transport. Since the dominant heat carriers for dielectric and semiconducting materials are phonons, which can have MFPs from nanometers up to several microns in materials such as silicon at room

*travis.frazer@colorado.edu

temperature [9–12], quasiballistic effects are observable in nanostructured systems, even at dimensions up to microns [13].

Observations of quasiballistic thermal transport have been made in several experimental geometries, including one-dimensional (1D) transport using transient grating experiments, ballistic transport through a thin slab of material whose thickness is shorter than the heat carrier's MFP, and also by measuring the transport away from nanoscale heat sources [10,13–16]. In this last category, the earliest experiments used effectively isolated heat sources to study thermal transport as a function of heat-source size. As the size of the heat source is decreased, a monotonic deviation from the Fourier prediction is observed due to the onset of quasiballistic transport. More recently, the study of nanoscale heat sources that are not isolated has revealed that not only the size of, but also the spacing between, heat sources impacts the nature of thermal transport [12,17–19]. In past work, we made the first observation of a collectively diffusive regime, where the thermal transport away from nanoscale hot spots can return toward the diffusive prediction when their spacing is reduced below the dominant heat-carrying phonon MFPs of the substrate [12]. This previously unobserved phenomenon has promising technological applications. We also developed a predictive, period- and linewidth-dependent theory for the effective resistivity, which predicted that the period, or line spacing, mattered. However, in our initial work, we did not independently vary both the heat-source size and spacing, or explore the transition between isolated and close-packed regimes, motivating the need for more systematic studies to benchmark advanced models and theories.

Here, we present a systematic study that independently controls the nanoscale heat-source size and spacing with laser-heated nanolines fabricated on silicon and fused-silica substrates. This allows us to definitively validate our surprising prediction that nanoscale heat sources whose separation is comparable to the phonon MFPs of the substrate should cool faster than identical heat sources that are spaced much farther apart [12]. Using an effective Fourier model, we quantify the enhancement of nanoscale thermal transport by engineering the heat-source spacing: for example, for a constant 20 nm-width nanoline, the isolated heat-source model [15] predicts an effective thermal boundary resistivity, r_{eff}, of 52 nK m^2/W, nanolines spaced by 400 nm have a measured r_{eff} of 9.2 nK m^2/W, nanolines spaced by 80 nm have a measured r_{eff} of 3.7 nK m^2/W, while the diffusive prediction for a uniform film is 2.45 nK m^2/W. Thus, the closely-packed nanolines exhibit thermal transport very close to diffusive, and varying their spacing makes it possible to significantly tune their transport properties. We also explore the transition from collective, close-packed transport to isolated, quasiballistic transport, which represents a broad parameter space that is important for optimized thermal design and for the development of full, first-principles models. Finally, we perform the same series of measurements on nanolines fabricated on a fused-silica-glass substrate, which exhibits no changes in transport as a function of either heat-source size or period. This behavior is expected: the phonon MFPs in fused silica are small compared to our experimental geometries, and thus heat transfer from these nanolines should be well described using a diffusive model. This measurement serves as a control to confirm that plasmonic or other effects in the nanolines do not influence our measurements. We also briefly discuss how these results compare to past results using different measurement techniques, as well as describing potential theories for the underlying transport mechanisms.

II. EXPERIMENTAL METHODS

A schematic of our experimental setup is shown in Fig. 1. We measure nanoscale thermal transport in silicon and fused silica using extreme ultraviolet (EUV) nanometrology, as described in Ref. [12]. For this study, the silicon and fused-silica substrates are patterned with periodic gratings of nickel nanolines via e-beam lithography. Using an ultrafast femtosecond laser pulse, we impulsively excite these nanostructures, which essentially serve as transducers for the thermal dynamics we measure. The excited thermal and acoustic dynamics deform the nanostructures and substrates, whose composite surface is then measured very sensitively using coherent-EUV

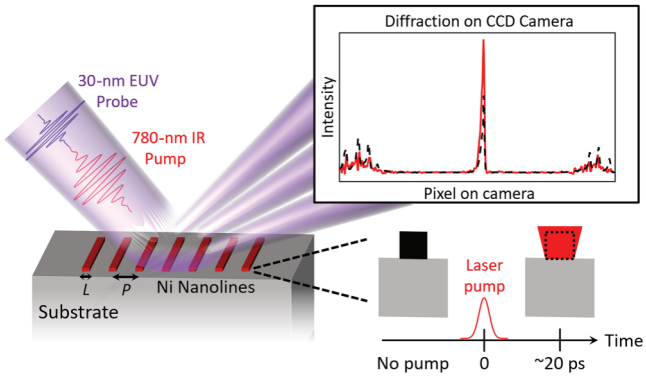

FIG. 1. EUV thermal and acoustic nanometrology. Gratings of nickel nanolines of linewidth L and period P are fabricated on silicon and fused-silica substrates. An ultrafast IR laser pulse heats the nanolines and they impulsively thermally expand (shown in lower right). An ultrafast EUV pulse then probes the sample as a function of time delay by measuring diffracted light using a CCD camera. The diffraction efficiency for a thermally excited sample (red in inset) changes compared to an unperturbed sample (black dotted line in inset). This change in diffraction efficiency captures the thermal and elastic dynamics that are deforming the sample surface. Note the change in the diffraction pattern shown is magnified 150× for illustration purposes.

beams generated by the high harmonic generation (HHG) process. See the Supplemental Material for a diagram of our laser system [20].

To explore the various nanoscale thermal-transport regimes, we choose grating linewidths and spacings that span from much smaller, to comparable, to greater than the average MFP, which is approximately 300 nm in silicon [12,21]. Therefore, we compare constant 25% duty-cycle gratings to constant period (varying duty cycle) gratings with linewidths ranging from 20 to 1000 nm. For the smallest linewidths (20–100 nm), the constant period is chosen to be 400 nm so that collective effects would still be present, but the reducing linewidth would probe the transition from the collectively diffusive regime to the isolated quasiballistic heat-source regime. Similarly, for linewidths from 100 to 300 nm, the constant period is 1500 nm, where collective effects should be much weaker. A complete list of gratings L and P characterized by AFM and SEM is given in the Supplemental Material [20]. By comparing results on these series of gratings, we directly measure the effect of heat-source spacing on nanoscale thermal transport. The constant period set of gratings produces increasingly isolated heat sources as the linewidth is decreased, whereas the constant duty cycle set of gratings brings the heat sources closer together as the linewidth is decreased. Each grating covers an area of 150 μm^2 and each nanoline is 11-nm tall on average [20,22].

We excite the nanolines using an ultrafast infrared laser pulse with a central wavelength of 780 nm, with a 25-fs pulse duration, and at a 4-kHz repetition rate [20]. The nickel gratings preferentially absorb the laser light, with no significant heat deposition in the substrate underneath: fused silica is transparent to this wavelength, while silicon has a >8 μm penetration depth. The nanolines are thinner than the optical penetration depth of Ni, ensuring uniform heating. After impulsive heating, the nanolines thermally expand within approximately 20 ps, launching acoustic waves that are visible in our raw data, as shown in Fig. 2. (In past work, these acoustic waves were used to characterize the elastic properties of ultrathin films [23,24].) After expanding, the Ni nanolines relax back to their unperturbed surface profile, as heat is transferred into the substrate on few nanoseconds time scales.

We use coherent EUV beams to directly measure changes in the nanosystem surface profile. We generate the EUV beams at a central wavelength of 29 nm through HHG [25]. This is an extreme nonlinear quantum process that up-converts IR light into the EUV region by focusing the laser pulse into an argon-filled waveguide. Since we use the same Ti:sapphire laser for both the excitation pulse and to generate the probe EUV pulse, the timing stability between our excitation and probe pulses is in the subfemtosecond range. In addition, EUV wavelengths are far from any electronic resonances in the nanosystem, so that the EUV reflectivity is largely insensitive to the electron temperature [26]. Thus, our technique predominantly probes lattice expansion and surface deformation, even for very short times after excitation (few picoseconds). The measured signal closely follows the lattice temperature of an average nanoline; this differs from the temperature difference measured by transient grating techniques, as shown in the Supplemental Material [20,27]. The diffracted EUV beam probes the dynamically changing sample surface, and is collected on a CCD camera, as shown in Fig. 1. The diffraction efficiency, that is, the relative power in the direct beam and diffracted orders, is a function of the height difference between the tops of the nanolines and the substrate. Thus, by monitoring the change in diffraction efficiency as a function of excitation-probe-delay time, we measure the thermal and elastic dynamics in both the nanolines and substrate with picometer-scale sensitivity (see Fig. 2 for an example) [26]. The delay between excitation and probe pulses is varied on timescales of up to 8 ns using a mechanical delay stage in the excitation laser's optical path. All measurements are performed at room temperature under high vacuum.

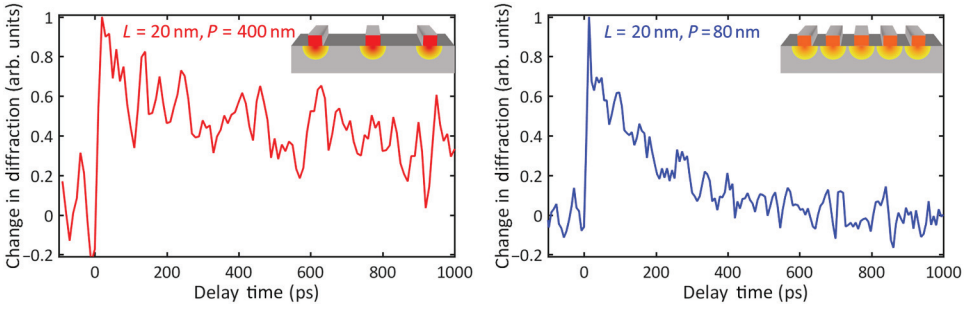

FIG. 2. Dynamically changing diffraction signals for 20-nm-linewidth gratings on silicon. The raw data directly show that closely spaced nanolines cool faster. Multifrequency acoustic oscillations in the substrate visibly modulate the slow-thermal decay of the signal. Left: 20-nm nanolines at a 400-nm period do not fully cool, even after 1 ns. Right: 20-nm nanolines at an 80-nm period have almost completely cooled within 1 ns.

We analyze the change in EUV diffraction efficiency signal by fitting with an effective Fourier model, implemented in the finite elements analysis (FEA) software, COMSOL [28,29]. FEA calculations use literature values for the nickel, silicon, and fused-silica properties, as listed in the Supplemental Material [12,15,20,30–39]. The thermal boundary resistivity at the nickel-substrate interface is taken as the effective fitting parameter. We simulate the thermal expansion and cooling of the nanolines for a variety of effective resistivities, and then calculate the diffraction of a Gaussian EUV beam from the dynamically changing surface using Fresnel propagation. The resulting calculated change in diffraction efficiency signal is then fit to the experimental signal to determine which effective resistivity best fits our experimental data. This effective resistivity contains both the intrinsic thermal boundary resistivity between the nanolines and the substrate, as well as an effective correction that is larger for greater deviations from diffusive thermal transport near the nanolines. The intrinsic thermal boundary resistivity should be constant across all gratings, independent of size and spacing, as all gratings on a given substrate are fabricated simultaneously. Therefore, trends in the best fit effective resistivity as a function of experimental geometry are due to the measured thermal transport's deviation from the diffusive prediction.

III. RESULTS AND DISCUSSION

First, we compare a series of gratings with constant period with another series of gratings with 25% duty cycle, both on a silicon substrate. For the 25% duty-cycle gratings, as the linewidth is decreased from 1000 to 20 nm, the effective resistivity first increases due to the quasiballistic deviation from diffusive transport, then decreases due to collective effects, as shown in Fig. 3(a) (blue points). At the smallest sizes, the effective resistivity approaches the diffusive, uniform heat-source limit, where there is only the intrinsic thermal-boundary resistivity, which has no effective correction due to nanoscale effects [black dashed line, Fig. 3(a)]. The reduction in effective resistivity occurs when the period becomes on the order of the dominant heat-carrying phonon MFPs in silicon at room temperature (approximately 300 nm). These findings are in good agreement with our previous work, as illustrated in Fig. 3(a), where we plot the collectively diffusive model developed by Hoogeboom-Pot, et al. (blue solid line) [12]. This collectively diffusive model relates each grating geometry to all the phonon modes' contributions to the thermal transport, according to the suppression function formalism [21,40]. The different MFP phonon modes' contributions to the total thermal conductivity are suppressed depending on the linewidth and reintroduced depending on the period of the grating. The suppression function is defined as

$$S(L,P,\Lambda)=\tanh\left(\frac{L}{2\Lambda}\right)+\left[1-\tanh\left(\frac{P}{2\Lambda}\right)\right], \quad (1)$$

where Λ is the MFP of a given phonon mode. Applying this suppression function to the bulk differential thermal-conductivity spectrum of the substrate, $k(\Lambda_i)$, we obtain an effective nanoscale conductivity for each grating geometry,

$$K_{\text{nano}}=\sum_i k(\Lambda_i)\cdot S(L,P,\Lambda_i), \quad (2)$$

where the sum is over each MFP mode, Λ_i. The model for the collectively diffusive effective resistivity is then defined by

$$r_{\text{eff}}=d\ln\left(\frac{P}{L}\right)\left(\frac{1}{K_{\text{nano}}}-\frac{1}{K_{\text{bulk}}}\right)+r_{\text{tbr}}, \quad (3)$$

where r_{tbr} is the intrinsic thermal-boundary resistivity, K_{bulk} is the bulk thermal conductivity of silicon, and d can be interpreted as the depth into the substrate where transport is affected by the nanoscale geometry.

As the grating period is increased for a fixed nanoline width, we would expect that thermal transport will become less efficient if the models developed in Ref. [12] are valid. Figure 3(a) plots the effective resistivity (red data points) as the period is increased from the collectively diffusive regime (blue data points). These values are seen to increase significantly when the period is increased, confirming model predictions. Considering now the trend in the red data points alone, the grating linewidth is reduced from 100 to 20 nm at a constant 400-nm period. Thus, the heat sources become increasingly isolated and the increasing effective resistivity maps the transition from collectively diffusive toward isolated quasiballistic transport. To successfully fit the 400-nm-period data, we use the collectively diffusive model described by Eqs. (1)–(3), applied to all the new data. As shown by the red dashed line in Fig. 3(a), this predictive model provides good fits, even in the intermediate regime, where heat sources are neither isolated nor closely spaced. Figure 3(a) also plots the isolated quasiballistic heat-source prediction for 1D gratings, as presented in Refs. [12,15], where no collective effects take place (black dotted line). This curve gives an upper limit to the transition region. This isolated, quasiballistic transport is described by the effective resistivity

$$r_{\text{isolated}}=\frac{4\Lambda_{\text{gray}}d}{3K_{\text{bulk}}(L/2)\ln(P/L)}+r_{\text{tbr}}, \quad (4)$$

where Λ_{gray} is the gray MFP approximation for the substrate (single, average MFP).

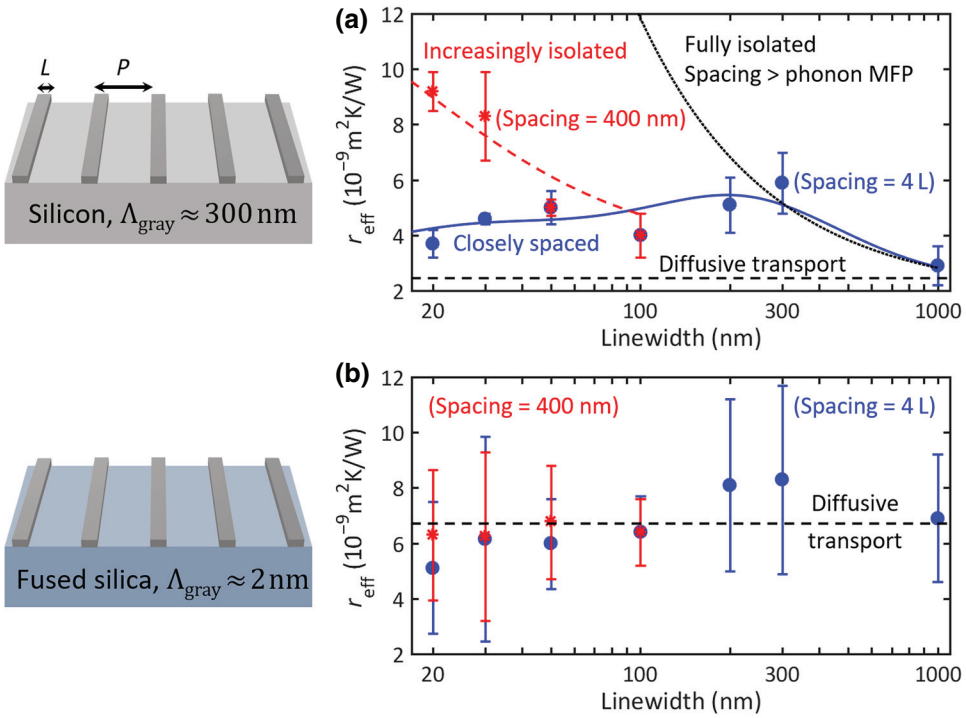

FIG. 3. Best fit effective thermal-boundary resistivity for nanolines on silicon and fused silica. (a) For silicon (gray MFP $\approx$ 300 nm [12,21]), as the linewidth is reduced below 50 nm, the effective resistivity of the constant 25% duty cycle gratings (blue points) decreases, which is a return toward the diffusive prediction (thin-film case, black dashed line). In contrast, the constant 400-nm-period gratings' resistivities increase as the linewidth is reduced (red points), mapping the transition from dominant collective effects toward isolated quasiballistic thermal transport (isolated prediction, black dotted line). The blue solid line is the 25% duty cycle collectively diffusive prediction from [12], whereas the red dashed line is a fit with the same model to the new data. (b) For fused silica, the resistivities of constant duty cycle (blue points) and 400-nm-period (red points) gratings all agree within error bars. This indicates that there is no nondiffusive transport that depends on experimental geometry for this short-phonon MFP material (approximately 2 nm [15]), and that there are no dominant systematic errors coming from the grating geometry independent of the sample substrate material. The dotted line is the average of all grating resistivities on fused silica (6.7 nK m^2/W). Error bars in (a) and (b) are calculated by the standard deviation of best fit values from multiple measurements.

These measurements on silicon represent the direct observation that the more closely spaced heat sources cool more quickly for sufficiently small periods at early times. At larger periods and linewidths, we do not observe this effect within our uncertainty, as shown in the Supplemental Material [20]. Our observed trends for different periods over the full range from 20- to 300-nm-linewidth gratings with the full effective Fourier analysis have not been previously reported and reveal that bringing heat sources closer together can bring the thermal transport within a factor of 2 of the diffusive prediction, even for heat-source sizes far below the dominant heat-carrying phonon MFPs. We further conclude that this effect is only dominant when grating periods are below the substrate MFPs, which is further supported by our control study on fused silica. We note that our best fit effective resistivities in the present work are close to the resistivity calculated from the corresponding thermal-boundary conductance measured by time-domain thermoreflectance (TDTR): 5.1 ± 0.3 nK m^2/W, converted from [41]. Some difference is expected due to differences in sample fabrication and the effective correction we add to the intrinsic thermal-boundary resistivity to capture nondiffusive effects in the substrate.

Next, we perform the same series of measurements on nanolines fabricated on a fused-silica-glass substrate, where the phonon MFPs (approximately 2 nm) are small compared to our experimental geometries, and therefore, no deviation from diffusive transport would be expected. The phonon MFPs of fused silica can be estimated as only a few nanometers at room temperature [15], and nonpropagating modes (diffusions) that contribute to the thermal conductivity should not be affected by our geometries [16,42]. Thus, these data serve as a control to confirm that plasmonic or other effects in the nanolines do not influence our Si measurements. Indeed, as shown in Fig. 3(b), the effective resistivity that best fits our data is constant, within error bars, for all linewidths and periodicities. It should be noted that the error bars for the fused-silica data, calculated from the standard deviation

of multiple measurements, are larger than in the silicon case due to two factors. First, experimental noise is larger, and second, our fitting has decreased sensitivity for low-conductivity samples where the thermal transport into the substrate is dominated by substrate conductivity rather than thermal-boundary resistivity. The thermal-boundary resistivities we fit for fused silica are consistent within error bars with previous measurements using this technique, with only a small offset we attribute to differences in the glass substrates and sample fabrication conditions [15].

Some care must be taken when comparing the results of the current study to TDTR measurements reported in the past on similar systems [17–19]. We note that this comparison can be beneficial for an improved understanding of the physics that is present in all three cases. Zeng *et al*. use periodic nanoline transducers at a variety of duty cycles. Their analysis shows that higher duty-cycle gratings have higher effective conductivities, which agrees with our direct observations. Hu *et al*. show results for two-dimensional (nanocube) gratings of constant period but decreasing linewidth, and observe a similar monotonic deviation from the bulk Fourier prediction we observe for that case. All three TDTR measurements differ from our results, however, in that they never observe a return toward the diffusive prediction at constant duty cycle, when the heat source period is comparable to the dominant substrate phonon MFPs. The reason for this difference might come from the different experimental temporal frequencies, as suggested by recent work by Hua and Minnich [43].

In their work, Hua and Minnich cast the Boltzmann transport equation (BTE) for phonons into the spatial-frequency domain and apply it to nanoscale-grating transducer geometries. They find that, due to the interplay of cross-plane and in-plane quasiballistic effects, thermal transport can indeed deviate from, and then return to, the diffusive prediction at constant duty cycle, but this will happen at smaller grating sizes for higher temporal frequencies of heating. For our EUV nanometrology measurements, we use a laser amplifier system to generate high harmonics at a few kilohertz repetition rate. In contrast, the TDTR measurements use laser oscillators with a repetition rate approximately equal to 80 MHz, modulated in the megahertz range as well. This difference might explain the difference between the EUV nanometrology and the TDTR measurements. Other theoretical approaches are in development that are also very promising for explaining our observed return toward the diffusive prediction, including hydrodynamic and superdiffusive views of the BTE that show lower temperatures near nanoscale heat sources than the temperature predicted by effective Fourier models [44–46]. In addition, potential coherent effects can modify the thermal transport in nanostructured systems, even at room temperature, via local resonances [6,7].

IV. CONCLUSION

We use ultrafast, coherent EUV beams to measure the thermal transport away from periodic gratings of laser-heated nickel nanolines with varying linewidth and spacing on both single-crystal silicon and amorphous fused-silica substrates. We observe quasiballistic transport that deviates from the diffusive prediction for nanolines on silicon and model this behavior with a higher effective thermal-boundary resistivity between the nanolines and the substrate. We observe that quasiballistically suppressed thermal transport returns toward the diffusive prediction when the nanoline spacing is comparable to the dominant phonon MFPs in the substrate. This period dependence confirms our previous prediction that closely spaced heat sources can initially cool faster than widely spaced ones and is now quantified to be a significant effect in silicon, bringing the thermal transport within a factor of 2 of the diffusive, uniform heat-source limit. Measurements on a fused-silica substrate displayed no quasiballistic behavior down to heat-source sizes of 20 nm. Our observations are in general agreement with other experimental and theoretical works. More work is needed to describe the fundamental physics behind these collective effects; the collectively diffusive model is a good first step that successfully describes real experimental geometries, but we are pursuing first-principles models to determine the fundamental mechanisms underlying these behaviors.

ACKNOWLEDGMENTS

The authors gratefully acknowledge support from the NSF STC on Real-Time Functional Imaging (STROBE): DMR 1548924, and a Gordon and Betty Moore Foundation EPiQS Award through Grant No.GBMF4538. J.K. acknowledges support from an SRC Graduate Fellowship. The authors acknowledge helpful discussions with Dr. Begoña Abad-Mayor.

[1] L. R. Hirsch, R. J. Stafford, J. A. Bankson, S. R. Sershen, B. Rivera, R. E. Price, J. D. Hazle, N. J. Halas, and J. L. West, Nanoshell-mediated near-infrared thermal therapy of tumors under magnetic resonance guidance, Proc. Natl. Acad. Sci. U.S.A. **100**, 13549 (2003).

[2] Z. Qin and J. C. Bischof, Thermophysical and biological responses of gold nanoparticle laser heating, Chem. Soc. Rev. **41**, 1191 (2012).

[3] Y. Lan, A. J. Minnich, G. Chen, and Z. Ren, Enhancement of thermoelectric figure-of-merit by a bulk nanostructuring approach, Adv. Funct. Mater. **20**, 357 (2010).

[4] P. Pichanusakorn and P. Bandaru, Nanostructured thermoelectrics, Mater. Sci. Eng. R **67**, 19 (2010).

[5] M. Maldovan, Sound and heat revolutions in phononics, Nature **503**, 209 (2013).

[6] B. L. Davis and M. I. Hussein, Nanophononic Metamaterial: Thermal Conductivity Reduction by Local Resonance, Phys. Rev. Lett. **112**, 055505 (2014).

[7] H. Honarvar, L. Yang, and M. I. Hussein, Thermal transport size effects in silicon membranes featuring nanopillars as local resonators, Appl. Phys. Lett. **108**, 263101 (2016).

[8] G. Chen, Nonlocal and nonequilibrium heat conduction in the vicinity of nanoparticles, J. Heat Transf. **118**, 539 (1996).

[9] K. Esfarjani, G. Chen, and H. T. Stokes, Heat transport in silicon from first-principles calculations, Phys. Rev. B **84**, 085204 (2011).

[10] J. A. Johnson, A. A. Maznev, J. Cuffe, J. K. Eliason, A. J. Minnich, T. Kehoe, C. M. S. Torres, G. Chen, and K. A. Nelson, Direct Measurement of Room-Temperature Nondiffusive Thermal Transport Over Micron Distances in a Silicon Membrane, Phys. Rev. Lett. **110**, 025901 (2013).

[11] J. Cuffe, J. K. Eliason, A. A. Maznev, K. C. Collins, J. A. Johnson, A. Shchepetov, M. Prunnila, J. Ahopelto, C. M. Sotomayor Torres, G. Chen, and K. A. Nelson, Reconstructing phonon mean-free-path contributions to thermal conductivity using nanoscale membranes, Phys. Rev. B **91**, 245423 (2015).

[12] K. M. Hoogeboom-Pot, J. N. Hernandez-Charpak, X. Gu, T. D. Frazer, E. H. Anderson, W. Chao, R. W. Falcone, R. Yang, M. M. Murnane, H. C. Kapteyn, and D. Nardi, A new regime of nanoscale thermal transport: Collective diffusion increases dissipation efficiency, Proc. Natl. Acad. Sci. U.S.A. **112**, 4846 (2015).

[13] A. J. Minnich, J. A. Johnson, A. J. Schmidt, K. Esfarjani, M. S. Dresselhaus, K. A. Nelson, and G. Chen, Thermal Conductivity Spectroscopy Technique to Measure Phonon Mean Free Paths, Phys. Rev. Lett. **107**, 095901 (2011).

[14] Y. K. Koh and D. G. Cahill, Frequency dependence of the thermal conductivity of semiconductor alloys, Phys. Rev. B **76**, 075207 (2007).

[15] M. E. Siemens, Q. Li, R. Yang, K. A. Nelson, E. H. Anderson, M. M. Murnane, and H. C. Kapteyn, Quasi-ballistic thermal transport from nanoscale interfaces observed using ultrafast coherent soft X-ray beams, Nat. Mater. **9**, 26 (2010).

[16] K. T. Regner, D. P. Sellan, Z. Su, C. H. Amon, A. J. H. McGaughey, and J. A. Malen, Broadband phonon mean free path contributions to thermal conductivity measured using frequency domain thermoreflectance, Nat. Commun. **4**, 1640 (2013).

[17] T. Oyake, M. Sakata, and J. Shiomi, Nanoscale thermal conductivity spectroscopy by using gold nano-islands heat absorbers, Appl. Phys. Lett. **106**, 073102 (2015).

[18] Y. Hu, L. Zeng, A. J. Minnich, M. S. Dresselhaus, and G. Chen, Spectral mapping of thermal conductivity through nanoscale ballistic transport, Nat. Nanotechnol. **10**, 701 (2015).

[19] L. Zeng, K. C. Collins, Y. Hu, M. N. Luckyanova, A. A. Maznev, S. Huberman, V. Chiloyan, J. Zhou, X. Huang, K. A. Nelson, and G. Chen, Measuring phonon mean free path distributions by probing quasiballistic phonon transport in grating nanostructures, Sci. Rep. **5**, 17131 (2015).

[20] See Supplemental Material at http://link.aps.org/supplemental/10.1103/PhysRevApplied.11.024042 for nanoline characterization, tables of parameters, discussion of measurement sensitivity, and further comparisons of our data.

[21] F. Yang and C. Dames, Mean free path spectra as a tool to understand thermal conductivity in bulk and nanostructures, Phys. Rev. B **87**, 035437 (2013).

[22] I. Horcas, R. Fernández, J. M. Gómez-Rodríguez, J. Colchero, J. Gómez-Herrero, and A. M. Baro, WSXM: A software for scanning probe microscopy and a tool for nanotechnology, Rev. Sci. Instrum. **78**, 013705 (2007).

[23] K. M. Hoogeboom-Pot, E. Turgut, J. N. Hernandez-Charpak, J. M. Shaw, H. C. Kapteyn, M. M. Murnane, and D. Nardi, Nondestructive measurement of the evolution of layer-specific mechanical properties in sub-10 nm bilayer films, Nano Lett. **16**, 4773 (2016).

[24] J. N. Hernandez-Charpak, K. M. Hoogeboom-Pot, Q. Li, T. D. Frazer, J. L. Knobloch, M. Tripp, S. W. King, E. H. Anderson, W. Chao, M. M. Murnane, H. C. Kapteyn, and D. Nardi, Full characterization of the mechanical properties of 11–50 nm ultrathin films: Influence of network connectivity on the Poisson's ratio, Nano Lett. **17**, 2178 (2017).

[25] A. Rundquist, C. G. Durfee, Z. Chang, C. Herne, S. Backus, M. M. Murnane, and H. C. Kapteyn, Phase-matched generation of coherent soft X-rays, Science **280**, 1412 (1998).

[26] R. I. Tobey, M. E. Siemens, O. Cohen, M. M. Murnane, H. C. Kapteyn, and K. A. Nelson, Ultrafast extreme ultraviolet holography: Dynamic monitoring of surface deformation, Opt. Lett. **32**, 286 (2007).

[27] H. J. Eichler, P. Günter, and D. W. Pohl, *Laser-Induced Dynamic Gratings* (Springer-Verlag Berlin Heidelberg, New York, 1986).

[28] COMSOL, Inc., *COMSOL Multiphysics, Version 4.3b* (COMSOL, Inc., Burlington, MA, 2013).

[29] F. Banfi, F. Pressacco, B. Revaz, C. Giannetti, D. Nardi, G. Ferrini, and F. Parmigiani, Ab initio thermodynamics calculation of all-optical time-resolved calorimetry of nanosize systems: Evidence of nanosecond decoupling of electron and phonon temperatures, Phys. Rev. B **81**, 155426 (2010).

[30] P. D. Desai, Thermodynamic properties of iron and silicon, J. Phys. Chem. Ref. Data **15**, 967 (1986).

[31] J. A. Dean and N. A. Lange, *Lange's Handbook of Chemistry* (McGraw-Hill, New York, NY, 1999), 15th ed.

[32] Y. S. Touloukian, *Thermophysical Properties of Matter: Vol 2. Thermal Conductivity – Nonmetallic Solids* (Plenum Publishing Corporation, New York, NY, 1970).

[33] D. Nardi, M. Travagliati, M. E. Siemens, Q. Li, M. M. Murnane, H. C. Kapteyn, G. Ferrini, F. Parmigiani, and F. Banfi, Probing thermomechanics at the nanoscale: Impulsively excited pseudosurface acoustic waves in hypersonic phononic crystals, Nano Lett. **11**, 4126 (2011).

[34] M. J. Weber, *Handbook of Optical Materials: Vol 3. Optical Materials, Part 1* (CRC Press, LLC, Boca Raton, FL, 2003).

[35] J. Zacharias, The Temperature Dependence of Young's Modulus for Nickel, Phys. Rev. **44**, 116 (1933).

[36] J. J. Wortman and R. A. Evans, Young's modulus, shear modulus, and Poisson's ratio in silicon and germanium, J. Appl. Phys. **36**, 153 (1965).

[37] T. G. Kollie, Measurement of the thermal-expansion coefficient of nickel from 300 to 1000 K and determination of the power-law constants near the Curie temperature, Phys. Rev. B **16**, 4872 (1977).

[38] Y. Okada and Y. Tokumaru, Precise determination of lattice parameter and thermal expansion coefficient of silicon between 300 and 1500 K, J. Appl. Phys. **56**, 314 (1984).

[39] Y. S. Touloukian, *Thermophysical Properties of High Temperature Solid Materials: Vol. 4. Oxides and Their Solutions and Mixtures* (The Macmillan Company, New York, NY, 1967).

[40] A. A. Maznev, J. A. Johnson, and K. A. Nelson, Onset of nondiffusive phonon transport in transient thermal grating decay, Phys. Rev. B **84**, 195206 (2011).

[41] R. Cheaito, J. T. Gaskins, M. E. Caplan, B. F. Donovan, B. M. Foley, A. Giri, J. C. Duda, C. J. Szwejkowski, C. Constantin, H. J. Brown-Shaklee, J. F. Ihlefeld, and P. E. Hopkins, Thermal boundary conductance accumulation and interfacial phonon transmission: Measurements and theory, Phys. Rev. B **91**, 035432 (2015).

[42] P. B. Allen and J. L. Feldman, Thermal conductivity of disordered harmonic solids, Phys. Rev. B **48**, 12581 (1993).

[43] C. Hua and A. J. Minnich, Heat dissipation in the quasiballistic regime studied using the Boltzmann equation in the spatial frequency domain, Phys. Rev. B **97**, 014307 (2018).

[44] P. Torres, A. Torelló, J. Bafaluy, J. Camacho, X. Cartoixà, and F. X. Alvarez, First principles kinetic-collective thermal conductivity of semiconductors, Phys. Rev. B **95**, 165407 (2017).

[45] A. Ziabari, P. Torres, B. Vermeersch, Y. Xuan, X. Cartoixà, A. Torelló, J.-H. Bahk, Y. R. Koh, M. Parsa, P. D. Ye, F. X. Alvarez, and A. Shakouri, Full-field thermal imaging of quasiballistic crosstalk reduction in nanoscale devices, Nat. Commun. **9**, 255 (2018).

[46] B. Vermeersch and N. Mingo, Quasiballistic heat removal from small sources studied from first principles, Phys. Rev. B **97**, 045205 (2018).